Virtual Three-Level Model Predictive Flux Control With Reduced Computational Burden and Switching Frequency for Induction Motors

Tao Jin, *Senior Member, IEEE*, Huiqing Song, Daniel Legrand Mon-Nzongo, *Member, IEEE*, Paul Gistain Ipoum-Ngome, *Member, IEEE*, Huangzheng Liao, and Minlong Zhu

***Abstract*— Model predictive flux control (MPFC) is an alternative control solution to the classic model predictive torque control (MPTC) for driving induction motors (IMs) without the complexity of tuning the weighting factors. However, when applied in motor drives fed by a two-level converter, it results in higher flux and torque ripples. To improve its performance, this article proposes a virtual three-level MPFC (V3-MPFC) method. The virtual vector method increases the total number of voltage vectors crucial for improving the closed-loop performances of the model predictive control. To reduce the computational burden, direct torque control and novel deadbeat (DB) control strategies are proposed. Compared with existing methods, the proposed DB-based method reduces V3-MPFC to a suboptimization problem and still ensures that the suboptimal solution is equivalent to the global optimal solution provided by V3-MPFC. In addition, the redundant states are exploited to lower the switching frequency (SF) without extending the cost function. The simulation and experiment results show that, compared with existing methods, the proposed strategy effectively reduces the flux and torque ripples, and requires a lower SF and execution time.**

***Index Terms*—Computational burden, induction motor (IM), suboptimization, switching frequency (SF), virtual three-level model predictive flux control (V3-MPFC).**

I. Introduction

In THE field of motor drives, induction motors (IMs) have attracted widespread attention because they generate high torque and allow easy maintenance [1]. In the last few decades, several control strategies have been developed for IMs. The field-oriented control (FOC) and direct torque control (DTC) are the standard and well-known closed-loop methods in academia and industry communities. Compared with FOC, DTC provides a fast torque response, but it has the disadvantages of large torque ripples and variable switching frequency (SF) [2].

In recent years, model predictive control (MPC) has been widely studied and successfully applied to motor drive applications since it offers several advantages, such as flexibility, simplicity, and fast closed-loop response [3].

In model predictive torque control (MPTC), the torque and flux are predicted for each of the eight candidate states generated by a two-level voltage source inverter (2L-VSI). These predictions are evaluated in the cost function which is then minimized for achieving the optimal state voltage to apply to the next sample [4], [5], [6]. Several modified MPTC methods are proposed in the literature for improving closed-loop performances and reducing the algorithm execution time. In the classic MPTC, the weighting factors (WFs) strongly influence the performance of the controller [4], [5], [6], [7]. To address the WF problem, the online tuning method [8], sequential MPC (SMPC) [9], and model predictive flux control (MPFC) are proposed [10], [11], [12]. In the MPFC, the torque and flux references are equivalently converted into a new flux reference vector. This allows the removal of the flux WF and simplification of the cost function to the flux control objective. The simplified flux control objective is used as the control criterion to select the optimal voltage vector (VV) [10], [11], [12]. The MPFC has been validated for providing good closed-loop performances; however, the limited number of states generated by a 2L-VSI limits the torque and flux accuracy. To reduce the torque and flux ripples, an effective solution is to increase the total number of VVs.

The virtual VV approach has been proposed to increase the number of states evaluated by MPC and address several control challenges without changing the converter topology. These challenges include the zero-sequence circulating current in the parallel inverters [13], the capacitor voltage imbalance issue in the three-level inverters [14], and closed-loop performance improvements [15]. In the Duty-MPTC, a virtual VV is generated by two different VVs [11], [16], [17]. In [11], two VVs are considered, and their duty ratios are calculated by minimizing the stator flux error. In [16] and [17], the duty ratio of active VV is obtained according to the principle of minimum torque

Manuscript received 22 June 2022; revised 4 September 2022; accepted 22 September 2022. Date of publication 28 September 2022; date of current version 18 November 2022. This work was supported in part by the Chinese National Natural Science Foundation under Grant 51977039 and in part by the Postdoctoral Science Foundation under Grant 283436. Recommended for publication by Associate Editor R. Kennel. *(Corresponding author: Tao Jin.)*

Tao Jin, Huiqing Song, Daniel Legrand Mon-Nzongo, Huangzheng Liao, and Minlong Zhu are with the School of Electrical Engineering and Automation, Fuzhou University, Fuzhou 350116, China (e-mail: jintly@fzu.edu.cn; 1647323492@qq.com; monnzongodaniel@yahoo.fr; 1594990909@qq.com; 200127181@fzu.edu.cn).

Paul Gistain Ipoum-Ngome is with the School of Electrical Engineering and Automation, Fuzhou University, Fuzhou 350116, China, and also with Pearl-Electric Co., Ltd., Guangzhou 511400, China (e-mail: ipoum24@yahoo.fr).

Color versions of one or more figures in this article are available at https://doi.org/10.1109/TPEL.2022.3210388.

Digital Object Identifier 10.1109/TPEL.2022.3210388

ripple and torque slope, respectively. Even though Duty-MPTC improves steady-state performance, it has a large computational burden. To mitigate the torque ripple and achieve a fixed SF, the space vector modulation (SVM) approach is associated with the MPC control strategy in [18].

A discrete space vector modulation (DSVM) technique was proposed in [12], [19], and [20]. In the DSVM approach, one sampling period is subdivided into N equal intervals where different real VVs are applied to obtain virtual VVs within the control period. However, DSVM generates several candidate VV (CVV) sequences, and the main challenge is to select a suitable solution for closed-loop control. For example, the preselection of the vector sequence affects the SF of the inverter. In addition, the use of the extended space vector of the inverter with virtual and real VVs increases the total number of iterations to predict the flux and evaluate the control objective; therefore, the resulting MPC requires a higher execution time.

To reduce the computational burden, several methods are proposed to limit the number of CVVs [20], [21], [22], [23], [24]. In the DTC approach, the CVVs to apply at each sample are obtained from the torque and flux deviation lookup tables (LUTs). DTC has a simple structure, provides a faster torque response, and better robustness against parameter changes. However, DTC generates higher torque and flux ripples, and the resulting SF is variable [2]. In [20], MPC evaluates only 12 of 37 VVs that verify the flux position, and torque and flux deviations. To reduce the number of CVVs to evaluate per sample, the LUTs based on flux and torque deviations are used in [21], [22], [23], and [24]. To further reduce the computational burden, the deadbeat (DB) technique selects the CVVs that satisfy the reference control voltage [18], [25], [26], [27]. Compared with MPC based on DTC approach, DB method provides a better steady-state and a similar fast transient response. MPFC based on DTC and DB methods are effective in reducing computational burden; however, it still provides higher torque and flux ripples when applied to a motor drive fed by 2L-VSI.

To improve MPFC performances under 2L-VSI, this article proposes a novel virtual vector method to extend the number of CVVs. To mitigate the computation burden, DTC and novel DB approaches are proposed to reduce the evaluation of MPFC to a sector and subsector, respectively. Among the two proposed MPFC approaches, the virtual three-level MPFC (V3-MPFC) based DB method is the most effective. It relies only on three VVs (3V3-MPFC) and still results in a suboptimal solution equal to the optimal solution provided by V3-MPFC based on the extended space vector (with all real and virtual states). The resulting 3V3-MPFC has the advantage of providing a better trade-off between driving performances and the operating SF without using any WFs. In addition, it has a lower computation burden which reduces the cost of the digital processor.

The rest of this article is organized into four sections. Section II presents the classic MPFC. Section III presents the proposed V3-MPFC based on six VVs (6V3-MPFC) and 3V3-MPFC approaches. The simulation and experimental validations of the proposed strategies are provided in Section IV and the conclusion is given in Section V.

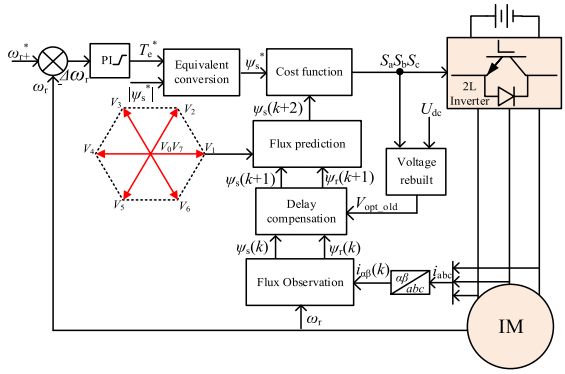

Fig. 1. MPFC control diagram of IM.

II. Model Predictive Flux Control

Fig. 1 presents the control diagram of MPFC, which consists of flux estimation, delay compensation, reference conversion, flux prediction, and cost function. The outer-loop controller based on proportional and integral generates the torque reference for the internal MPC controller.

A. IM Model

In the orthogonal reference, the dynamic model of the IM in continuous time is given by

$$v_{\mathrm{s}} = p\psi_{\mathrm{s}} + R_{\mathrm{s}} i_{\mathrm{s}} \tag{1}$$

$$0 = R_{\mathrm{r}} i_{\mathrm{r}} + p\psi_{\mathrm{r}} - j\omega_{\mathrm{r}}\psi_{\mathrm{r}} \tag{2}$$

$$\psi_{\mathrm{s}} = L_{\mathrm{s}} i_{\mathrm{s}} + L_{\mathrm{m}} i_{\mathrm{r}} \tag{3}$$

$$\psi_{\mathrm{r}} = L_{\mathrm{m}} i_{\mathrm{s}} + L_{\mathrm{r}} i_{\mathrm{r}} \tag{4}$$

$$T_{\mathrm{e}} = 1.5 n_{\mathrm{p}} \{\psi_{\mathrm{s}} \otimes i_{\mathrm{s}}\}. \tag{5}$$

From (1) to (4), the equivalent dynamic model coupling the stator and rotor of the IM is given by

$$i_{\mathrm{s}} + \tau_\sigma p i_{\mathrm{s}} = k_{\mathrm{r}}(1/\tau_{\mathrm{r}} - j\omega_{\mathrm{r}})\psi_{\mathrm{r}} / R_\sigma + v_{\mathrm{s}} / R_\sigma \tag{6}$$

$$\psi_{\mathrm{r}} + \tau_{\mathrm{r}} p\psi_{\mathrm{r}} = -j\omega_{\mathrm{r}}\tau_{\mathrm{r}}\psi_{\mathrm{r}} + L_{\mathrm{m}} i_{\mathrm{s}} \tag{7}$$

where $\otimes$ represents the cross product, $p = d/dt$ is the differential operator, R_{r} and R_{s} are the rotor and stator resistances, T_{e} is the electromagnetic torque, v_{s} and i_{s} are the stator voltage and current, i_{r} is the rotor current, L_{s}, L_{r}, and L_{m} are the stator, rotor, and mutual inductances, ψ_{s} and ψ_{r} are the stator and the rotor flux, and ω_{r} is the rotor electrical speed. n_{p} is the number of pole pairs, $\sigma = 1\text{-}L_{\mathrm{m}}{}^2/(L_{\mathrm{s}}L_{\mathrm{r}})$ is the leakage inductance coefficient, $\tau_{\mathrm{r}} = L_{\mathrm{r}}/R_{\mathrm{r}}$, $k_{\mathrm{r}} = L_{\mathrm{m}}/L_{\mathrm{r}}$, $R_\sigma = R_{\mathrm{s}} + R_{\mathrm{r}} k_{\mathrm{r}}{}^2$, $\tau_\sigma = \sigma L_{\mathrm{s}}/R_\sigma$.

B. Flux Estimation and Prediction

In [12], the rotor flux at k sample is based on the stator current and the previous rotor flux, and it is given by

$$\psi_{\mathrm{r}}(k) = \left(1 - \frac{T_{\mathrm{s}}}{\tau_{\mathrm{r}}}\right)\psi_{\mathrm{r}}(k-1) + \frac{L_{\mathrm{m}} T_{\mathrm{s}} i_{\mathrm{s}}(k)}{\tau_{\mathrm{r}}} - j\omega_{\mathrm{r}} T_{\mathrm{s}} \psi_{\mathrm{r}}(k-1). \tag{8}$$

Thus, using the measured speed and stator current in the orthogonal reference, the rotor flux is estimated in (8). By substituting (4) into (3), the relationship between the stator and rotor flux is given by

$$\psi_{\mathrm{s}}(k) = L_{\mathrm{m}}(\psi_{\mathrm{r}}(k) - L_{\mathrm{m}} i_{\mathrm{s}}(k))/L_{\mathrm{r}} + L_{\mathrm{s}} i_{\mathrm{s}}(k). \tag{9}$$

In practice, the digital controller has a one-sample time delay, which negatively affects the accuracy of the controller. To compensate for the time delay, a two-step prediction is required. According to [5], the stator current, electromagnetic torque, and stator flux at k+1 sample are given by

$$i_{\mathrm{s}}(k+1) = (k_{\mathrm{r}}(1 - j\omega_{\mathrm{r}}\tau_{\mathrm{r}})\psi_{\mathrm{r}}(k) + \tau_{\mathrm{r}} V_{\mathrm{opt\_old}}) \times T_{\mathrm{s}}/(\tau_\sigma R_\sigma \tau_{\mathrm{r}}) + (1 - T_{\mathrm{s}}/\tau_\sigma) i_{\mathrm{s}}(k) \tag{10}$$

$$\psi_{\mathrm{s}}(k+1) = \psi_{\mathrm{s}}(k) + T_{\mathrm{s}} V_{\mathrm{opt\_old}} - R_{\mathrm{s}} T_{\mathrm{s}} i_{\mathrm{s}}(k) \tag{11}$$

$$\psi_{\mathrm{r}}(k+1) = L_{\mathrm{r}}\psi_{\mathrm{s}}(k+1)/L_{\mathrm{m}} + (L_{\mathrm{m}}^2 - L_{\mathrm{r}}L_{\mathrm{s}}) i_{\mathrm{s}}(k+1)/L_{\mathrm{m}} \tag{12}$$

where $V_{\mathrm{opt\_old}}$ is the VV applied at sampling instant k. The state vectors at time k+1 are used as inputs for predicting the stator flux, stator current, and electromagnetic torque [5]. The expressions are given by

$$\psi_{\mathrm{s}}(k+2) = \psi_{\mathrm{s}}(k+1) + T_{\mathrm{s}} v_{\mathrm{s\_i}} - R_{\mathrm{s}} T_{\mathrm{s}} i_{\mathrm{s}}(k+1) \tag{13}$$

$$i_{\mathrm{s}}(k+2) = (k_{\mathrm{r}}(1 - j\omega_{\mathrm{r}}\tau_{\mathrm{r}})\psi_{\mathrm{r}}(k+1) + \tau_{\mathrm{r}} v_{\mathrm{s\_i}}) \times T_{\mathrm{s}}/\tau_\sigma R_\sigma \tau_{\mathrm{r}} + (1 - T_{\mathrm{s}}/\tau_\sigma) i_{\mathrm{s}}(k+1) \tag{14}$$

$$T_{\mathrm{e}}(k+2) = 1.5 n_{\mathrm{p}} \{\psi_{\mathrm{s}}(k+2) \otimes i_{\mathrm{s}}(k+2)\} \tag{15}$$

where $v_{\mathrm{s\_i}} \in \{V_0, V_1, \ldots, V_7\}$ is a CVV generated by a 2L-VSI. Depending on the control target, the predicted states given in (13)–(15) are evaluated to obtain the optimal control action for the next sample.

C. Flux Control Objective

In the classic MPTC, the torque and stator flux control objectives are evaluated to obtain the optimal control state [4], [5], [6]. In this regard, the cost function is given by

$$J = |T_{\mathrm{e}}^* - T_{\mathrm{e}}(k+2)| + k_\psi \, ||\psi_{\mathrm{s}}^*| - |\psi_{\mathrm{s}}(k+2)|| \tag{16}$$

where T_{e}^* and $|\psi_{\mathrm{s}}^*|$ are the torque and stator flux references, respectively. k_ψ is the flux WF, which defines the control importance between the torque and flux control objectives. A large value of k_ψ prioritizes the tracking of the flux over the torque which results in higher torque ripple and vis-versa. Unfortunately, the tuning of k_ψ is not trivial, due to the lack of analytical design procedures [8], [9], [10], [11], [12]. In addition, it is challenging to obtain a suited WF for a wide operating range.

To avoid tuning the flux WF, the multiobjective cost function is converted into a single control objective by evaluating the predicted stator flux as a function of the desired torque. Using the relation between the torque, stator, and rotor flux of IM, the electromagnetic torque is derived as follows:

$$T_{\mathrm{e}} = 1.5 n_{\mathrm{p}} \frac{L_{\mathrm{m}}}{L_{\mathrm{s}} L_{\mathrm{r}} \sigma} \psi_{\mathrm{r}} \otimes \psi_{\mathrm{s}} = 1.5 n_{\mathrm{p}} \frac{L_{\mathrm{m}}}{L_{\mathrm{s}} L_{\mathrm{r}} \sigma} |\psi_{\mathrm{r}}| \, |\psi_{\mathrm{s}}| \sin(\angle\psi_{\mathrm{s}} - \angle\psi_{\mathrm{r}}). \tag{17}$$

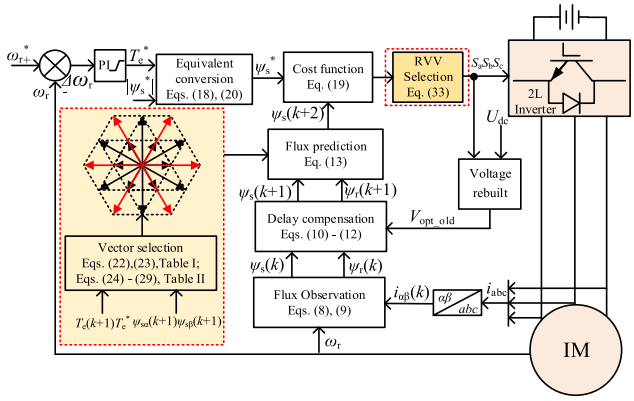

Fig. 2. Control diagram of the proposed V3-MPFC.

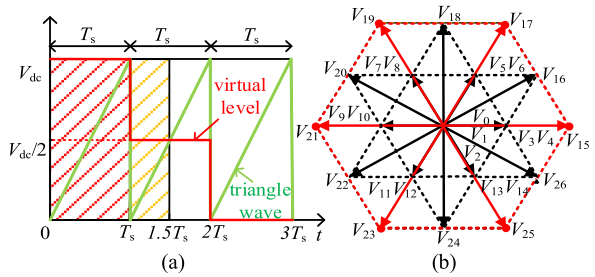

Fig. 3. Principle for generating a virtual space vector. (a) Implementation of real and virtual voltages. (b) Virtual three-level space vector.

From (17), the phase shift relationship between stator flux and rotor flux is derived. The DB control method is used to derive the stator flux vector reference, which can be expressed as a function of T_{e}^* and $|\psi_{\mathrm{s}}^*|$ [10], [11], [12]. For time delay compensation, the predicted rotor flux at k+1 is considered, and the reference angle of the stator flux is given by

$$\angle\psi_{\mathrm{s}}^* = \angle\psi_{\mathrm{r}}^{\mathrm{k+1}} + \sin^{-1}\left(\frac{2 L_{\mathrm{s}} L_{\mathrm{r}} \sigma T_{\mathrm{e}}^*}{3 n_{\mathrm{p}} L_{\mathrm{m}} \left|\psi_{\mathrm{r}}^{\mathrm{k+1}}\right| |\psi_{\mathrm{s}}^*|}\right). \tag{18}$$

Since the new stator flux reference is obtained based on the desired torque, the cost function in (16) is simplified to the flux control objective as given by

$$J = |\psi_{\mathrm{s}}^* - \psi_{\mathrm{s}}(k+2)| \tag{19}$$

where the new stator flux reference is given by

$$\psi_{\mathrm{s}}^* = |\psi_{\mathrm{s}}^*| \, \mathrm{e}^{j\angle\psi_{\mathrm{s}}^*}. \tag{20}$$

MPFC has been validated for providing good performances in motor drives, but it still generates higher torque and flux ripples when the evaluation of the MPFC is limited to the eight discrete states generated by a 2L-VSI [10]. To further improve the closed-loop performances, one alternative solution is to increase the number of states considered during the evaluation of MPC [12], [19], [20], [26].

III. Proposed V3-MPFC

The diagram of the proposed V3-MPFC is presented in Fig. 2. Compared with the classic MPFC using a two-level space vector,

the proposed method uses a virtual three-level space vector to improve the closed-loop performances. The DTC or a novel DB scheme is included in the algorithm to operate the MPFC controller within a subspace of the virtual VV, therefore, reducing the algorithm computational burden.

A. Virtual Three-Level Space Vector

For a three-phase 2L-VSI, each phase generates up to two voltage levels which are zero and $V_{\rm dc}$, where $V_{\rm dc}$ is the dc voltage. For a three-phase inverter, the total number of CVVs is equal to 8. With a limited number of states, MPFC produces relatively high stator flux and torque ripples [10]. To reduce the flux and torque ripples under 2L-VSI, the number of CVVs for prediction is increased by using the virtual vector method.

To expand the converter to operate not only at the edge of its operating region but also in the linear region, the virtual VVs are generated by applying multiple real states within a control period and controlling their duration [12], [16], [17], [18], [19], [20], [26]. In the Duty-MPTC, the duty ratios of the two applied states are calculated by minimizing the stator flux error or the torque slope [16], [17]. The DSVM method is used to reduce the flux and torque ripples [12], [20], [26]. To discretize the space vector of 2L-VSI into a virtual multilevel inverter, one sampling period is subdivided into *N* equal intervals where different real VVs are applied to generate a virtual VV.

Without redundant VVs (RVVs), the total number of VVs which includes real and virtual VVs is calculated as given by

$$n_{\rm total} = 3N^2 + 3N + 1. \tag{21}$$

For $N = 2$, the total number of VVs is 19 [12], [20], [26].

In classic MPC, basic VVs are applied during the entire control period $T_{\rm s}$, as illustrated during [0, $T_{\rm s}$] and [2$T_{\rm s}$, 3$T_{\rm s}$] in Fig. 3(a). In this article, to expand a two-level space vector into a virtual three-level space vector, the synthesized virtual VVs are based on zero-voltage and active-voltage, as illustrated during [$T_{\rm s}$, 2$T_{\rm s}$] in Fig. 3(a). For example, to generate VV V_4 (0.50,0), the real VVs V_{15} and V_0 are applied during a period of 0.5$T_{\rm s}$ and 0.5$T_{\rm s}$, respectively. The resulting virtual three-level space vector consists of 27 states, which includes eight real and 19 virtual VVs as presented in Fig. 3(b).

Using an extended virtual three-level space vector in MPFC has the advantage of reducing flux and torque ripples compared with the traditional MPFC method relying on eight VVs. Considering the converter is two-level, RVVs can be avoided and still achieve good performances. Even without RVVs, the remaining 19 CVVs are still larger than eight, therefore, the computational burden of V3-MPFC is expected to be higher than under the traditional MPFC. To implement the V3-MPFC algorithm in a low-cost processor, it is vital to reduce the number of states used for closed-loop at each sample.

B. Prediction of CVVs for Closed-Loop Control

To reduce the control problem to a subspace with a limited number of states evaluated at each sample, DTC and novel DB approaches are proposed. With the DTC method, the extended space vector presented in Fig. 3(b) is reduced to a sector and a subsector with the proposed DB approach.

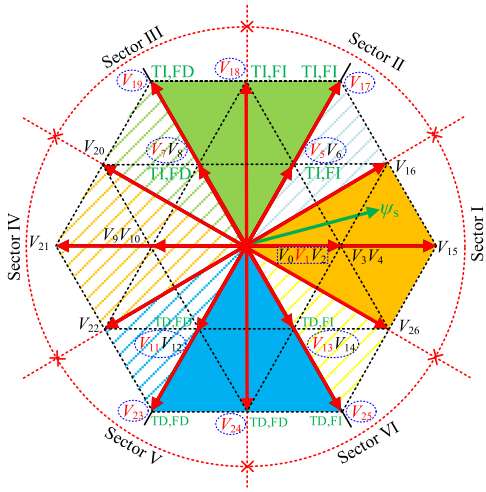

Fig. 4. VVs selection based on DTC method.

1) Approach #1. Prediction of CVVs Within a Sector: The distribution of the VVs in the α–β frame is shown in Fig. 4. For 2L-VSI, the converter region is divided into six sectors, each containing zero and active VVs. With the virtual space vector, the converter operating region is also divided into six sectors, but each sector consists of zero, small, medium, and large VVs. The relationship between angle and sector is given by

$$(2M-3)\pi/6 \le \theta(M) \le (2M-1)\pi/6 \tag{22}$$

where θ(M) is the angle of sector *M*, where 1≤M≤6.

In [23], the DTC method is used for reducing the number of CVVs from a two-level space vector to a sector at each sample. The CVVs for the next sample are predicted by using the angle of the stator flux and either the flux or torque deviation. The stator flux $\psi_{\rm s}$ ($\psi_{{\rm s}\alpha}$, $\psi_{{\rm s}\beta}$) angle is calculated as given by

$$\theta_{\psi_{\rm s}} = \arctan(\psi_{{\rm s}\beta}/\psi_{{\rm s}\alpha}). \tag{23}$$

With MPFC based on the DTC method, the candidate states are within the predicted sector. For example, to obtain the VVs to be evaluated by MPFC, the stator flux is initially considered in sector I at *k* sample. With the torque deviation $dT_{\rm e} > 0$, $dT_{\rm e} = T_{\rm e}^*–T_{\rm e}$, the VVs satisfying torque increase, and flux increase or decrease (FI or FD) are located in the green region. Since each small VV has an RVV, the CVVs for MPFC closed-loop are V_1, V_5, V_7, V_{17}, V_{18}, and V_{19}. Similarly, if the torque deviation is $dT_{\rm e} < 0$, the VVs satisfying torque decrease are located in the blue region, and includes V_1, V_{11}, V_{13}, V_{23}, V_{24}, and V_{25}. When the torque deviation $dT_{\rm e} = 0$, the zero vector V_1 is the CVV. Using the same principle, when the stator flux is located in other sectors, the CVVs evaluated at each sample are determined according to Table I. However, in the DTC method, the resulting SF is variable, and a complex LUT is required as the number of states increases.

TABLE I
CVVs BASED ON DTC

	Sector	CVVs
$dT_e = 0$		V_1
$dT_e > 0$	I	$V_1, V_5, V_7, V_{17}, V_{18}, V_{19}$
	II	$V_1, V_7, V_9, V_{19}, V_{20}, V_{21}$
	III	$V_1, V_9, V_{11}, V_{21}, V_{22}, V_{23}$
	IV	$V_1, V_{11}, V_{13}, V_{23}, V_{24}, V_{25}$
	V	$V_1, V_{13}, V_{15}, V_{25}, V_{26}, V_{15}$
	VI	$V_1, V_3, V_5, V_{15}, V_{16}, V_{17}$
$dT_e < 0$	I	$V_1, V_{11}, V_{13}, V_{23}, V_{24}, V_{25}$
	II	$V_1, V_{13}, V_3, V_{15}, V_{25}, V_{26}$
	III	$V_1, V_3, V_5, V_{15}, V_{16}, V_{17}$
	IV	$V_1, V_5, V_7, V_{17}, V_{18}, V_{19}$
	V	$V_1, V_7, V_9, V_{19}, V_{20}, V_{21}$
	VI	$V_1, V_9, V_{11}, V_{21}, V_{22}, V_{23}$

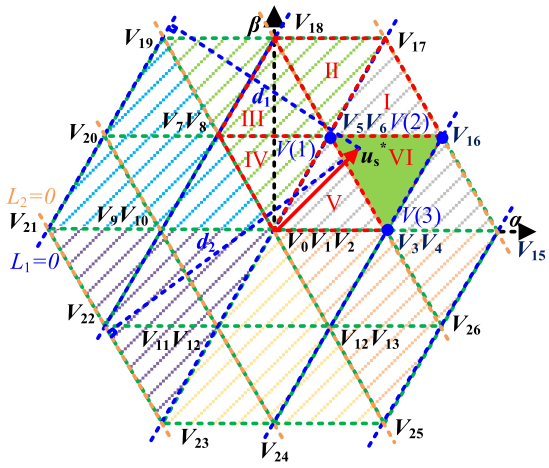

Fig. 5. VVs selection based on DB method.

2) Approach #2. Prediction of CVVs Within a Subsector: In [26], the stator voltage reference is used to reduce the closed-loop control to a suboptimization problem. Considering the stator flux is a linear function of the stator voltage, the reference control VV associated with the flux reference is derived by

$$u_s^* = (\psi_s^* - \psi_s(k+1))/T_s + R_s i_s(k+1). \tag{24}$$

With the reference control VV, the control problem is reduced from a virtual space vector to a subsector as illustrated in Fig. 5. To limit the reference control voltage within the boundaries of the inverter operating region, $u_s{}^*$ is constrained as given by

$$u_s^* = \begin{cases} \frac{u_s^*}{|u_s^*|}\,|v_{s\max}| & |u_s^*| > |v_{s\max}| \\ u_s^* & |u_s^*| \le |v_{s\max}| \end{cases}. \tag{25}$$

where $|v_{s\max}|$ is the maximum magnitude of the space vector.

For each sample, the reference VV is within a subsector, this subsector contains VVs with the smallest distance to the reference VV. The subsector can be obtained by online evaluation of each distance from the end point of the reference VV to the CVVs. However, such extensive evaluation has the potential to increase the computational burden of the control algorithm. An alternative solution that requires less execution time is the DB approach. With the DB method, the boundaries of all subsectors

TABLE II
TABLE OF CVVs FOR EVALUATION

Sector	Vector	Sector	Vector
I	①, ②	IV	④, ⑤
II	②, ③	V	⑤, ⑥
III	③, ④	VI	⑥, ①

and the coordinates of the reference VV are used to select the subsector which borders the reference VV. The DB method proposed in [26] requires three axes for projection to locate the subsector solution with the reference VV. To reduce the design complexity, the newly proposed DB uses only two axes to locate the subsector.

By considering d_1 and d_2 as the distance from the end point of the reference VV $u_s{}^*$ to the axes $L_1 = 0$ and $L_2 = 0$, the expressions of the distance d_1 and d_2 are given by

$$\begin{cases} d_1 = \left|\sqrt{3}u_{s\beta}^* - 3u_{s\alpha}^* - 2V_{dc}\right|/V_{dc} \\ d_2 = \left|\sqrt{3}u_{s\beta}^* + 3u_{s\alpha}^* + 2V_{dc}\right|/V_{dc}. \end{cases} \tag{26}$$

By rounding d_1 and d_2, the results are denoted as D_1 and D_2. The expressions of $V(1)$ and the voltage error V_{error} between $V(1)$ and the reference VV are given by

$$V(1) = \frac{((D_1 + D_2 - 4) + j\sqrt{3}(D_2 - D_1))}{(6/V_{dc})} \tag{27}$$

$$V_{error} = V(1) - u_s^*. \tag{28}$$

By using (28), the subsector with $V(1)$, $V(2)$, and $V(3)$ is determined. Within a subsector, the unknown other VVs $V(2)$ and $V(3)$ are calculated according to (29) and Table II.

For example, when $u_s{}^*$ is located in the subsector VI as shown in Fig. 5, $V(1)$ is obtained according to (27), while $V(2)$ and $V(3)$ are obtained from ⑥ and ① in the following equation:

$$\begin{cases} V = V(1) + V_{dc}/3 & ① \\ V = V(1) + (1 + j\sqrt{3})V_{dc}/6 & ② \\ V = V(1) + (-1 + j\sqrt{3})V_{dc}/6 & ③ \\ V = V(1) - V_{dc}/3 & ④ \\ V = V(1) - (1 + j\sqrt{3})V_{dc}/6 & ⑤ \\ V = V(1) - (-1 + j\sqrt{3})V_{dc}/6 & ⑥ \end{cases}. \tag{29}$$

The resulting number of CVVs under the proposed DB method is equal to 3, which is smaller than the 6 obtained under method #1. Therefore, 3V3-MPFC is expected to have a lower computational burden compared with 6V3-MPFC.

The proposed DB method reduces the MPFC closed-loop problem to a subspace, and the suboptimal solution achieved is equal to the solution provided by V3-MPFC. Considering that the stator flux in (13) depends on the inverter control voltage, the predicted and reference stator flux can be rewritten

$$\psi_s(k+2) = av_{s\_i} + b \tag{30}$$

$$\psi_s^* = au_s^* + b \tag{31}$$

where $a = T_s$ and $b = \psi_s(k+1)$-$R_s T_s i_s(k+1)$.

Using (30) and (31), the flux control objective given in (19) is simplified to the voltage control objective as given by

$$J = |\psi_{\mathrm{s}}^{*} - \psi_{\mathrm{s}}(k+2)| = a|u_{\mathrm{s}}^{*} - v_{\mathrm{s\_i}}|. \tag{32}$$

The optimum control voltage which is a VV with the smallest distance to the reference voltage can be achieved by exhaustive evaluation of (32). V3-MPFC evaluates 19 CVVs to obtain the optimal vector which is equivalent to the control voltage with the smallest distance to the reference voltage obtained by using the proposed DB method. For instance, with the reference control vector presented in Fig. 5, V_5 and V_6 are the redundant optimal vectors resulting from the evaluation of (19) and they are the same vectors obtained by using (24)–(29), and Table II.

C. Average SF Reduction Scheme

The RVVs are used to reduce the average SF (ASF), which is decisive in lowering the inverter switching losses. In this work, when the optimal state is small or zero VV, the optimal RVV applied to the next sample is the one with lower ASF, and ASF is given by

$$\mathrm{ASF} = \frac{1}{6}\sum_{n=a,b,c}\sum_{i=1}^{2}\mathrm{ASF}_{ni}. \tag{33}$$

For example, considering V_{23} ($S_{\mathrm{a}}=0$, $S_{\mathrm{b}}=0$, $S_{\mathrm{c}}=1$) as the previous applied state voltage, V_{11} ($S_{\mathrm{a}}=0.5$, $S_{\mathrm{b}}=0.5$, $S_{\mathrm{c}}=1$) and V_{12} ($S_{\mathrm{a}}=0$, $S_{\mathrm{b}}=0$, $S_{\mathrm{c}}=0.5$) are CVVs satisfying the flux control objective, the optimal VV with lower ASF in the next sample is V_{12} ($S_{\mathrm{a}}=0$, $S_{\mathrm{b}}=0$, $S_{\mathrm{c}}=0.5$). Using a similar approach for zero VVs, the optimal redundant zero VV is the one with a lower switching commutation. Without extending the cost function, the insertion of the ASF scheme is expected to significantly mitigate the switching losses.

D. Proposed Control Algorithm

The proposed control strategy is presented in Fig. 6. The control procedure is summarized by the following steps.

Step 1) Measurement: sample $i_{\mathrm{a}}(k)$, $i_{\mathrm{b}}(k)$, $i_{\mathrm{c}}(k)$, ω_{r}.
Step 2) Apply: apply the previous optimal VV $V_{\mathrm{opt\_old}}$.
Step 3) Estimate: estimate rotor flux $\psi_{\mathrm{r}}(k)$ and stator flux $\psi_{\mathrm{s}}(k)$ using (8) and (9), respectively.
Step 4) Delay compensation: calculate stator current $i_{\mathrm{s}}(k+1)$, the stator flux $\psi_{\mathrm{s}}(k+1)$, and rotor flux $\psi_{\mathrm{r}}(k+1)$ using (10), (11), and (12), respectively.
Step 5) Desired stator flux vector: obtain the desired stator flux vector $\psi_{\mathrm{s}}{}^{*}$ by using (18) and (20).
Step 6) CVVs selection: for 6V3-MPFC, the CVVs for evaluation are chosen based on (22), (23), and Table I. While for 3V3-MPFC, the CVVs are chosen according to (24)–(29), and Table II.
Step 7) Prediction: use (13) to predict the flux at $k+2$ for the CVVs selected in step 6.
Step 8) Optimization: evaluate the cost function (19) for the CVVs and select the optimal VV that minimizes the cost function.

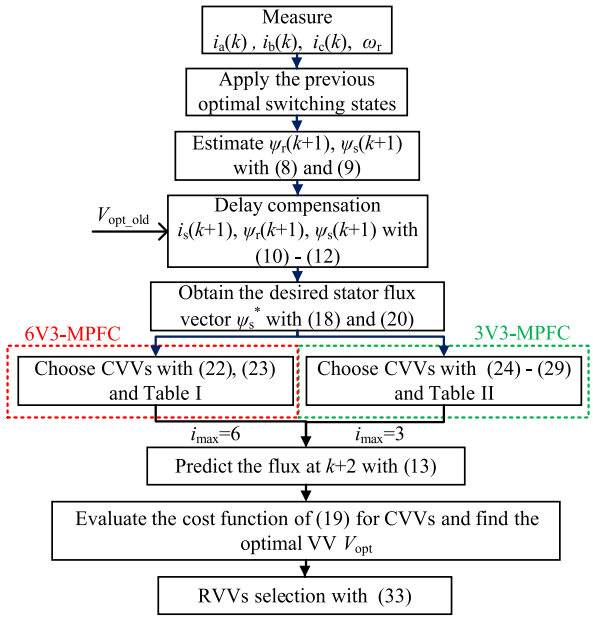

Fig. 6. Algorithm of the proposed 6V3-MPFC and 3V3-MPFC control strategies.

TABLE III
MOTOR AND INVERTER PARAMETERS

Variables	Parameters	Values
V_{dc}	DC link voltage	520 V
P_N	Rated power	3 kW
U_N	Rated voltage	380 V
f_N	Rated frequency	50 Hz
T_N	Rated torque	20 Nm
N_p	Number of pole pairs	2
R_s	Stator resistance	3.15 Ω
R_r	Rotor resistance	1.1 Ω
L_m	Mutual inductance	0.25 H
L_s	Stator inductance	0.2552 H
L_r	Rotor inductance	0.2578 H
$\lvert\psi_s^*\rvert$	Flux amplitude reference	0.71 Wb
f_s	Sampling frequency	10 kHz

Step 9) RVVs selection: if the optimal VV is RVV, select the one with the lower ASF by using (33).

IV. Simulation and Experimental Verification

For simulation and experimental validations, the parameters of 2L-VSI and IM are given in Table III. For comparative study, the classic MPFC [10], the DSVM-DTC ($N=2$) method [20], and the proposed 6V3-MPFC and 3V3-MPFC are evaluated.

The cost function values of various controllers are used to evaluate the optimality. A suboptimization occurs if the cost function value produced by a simplified method is higher than the one provided by the conventional method. If the cost function values are the same, the suboptimality is zero, in this scenario, both controllers will provide the same steady-state and dynamic performance [12]. In summary, the suboptimality parameter is

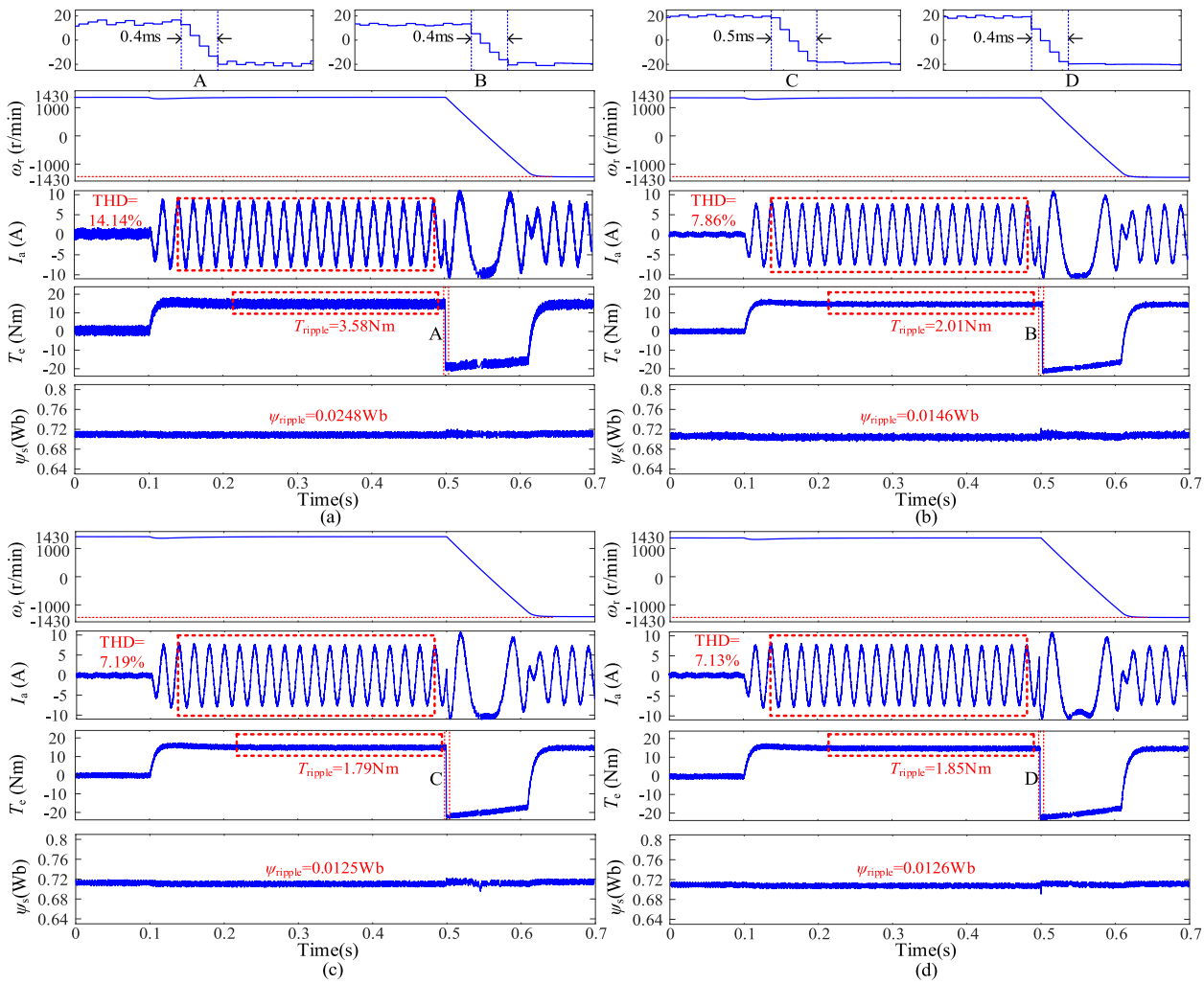

Fig. 7. Simulation results of IM speed, A-phase current, torque, and stator flux waveform. (a) MPFC. (b) DSVM-DTC ($N = 2$). (c) 6V3-MPFC. (d) 3V3-MPFC.

defined by

$$Suboptimality = \begin{cases} 0 & if\ |\Delta J| = 0 \\ 1 & otherwise \end{cases} \tag{34}$$

where $|\Delta J| = |J\text{-}J_{\text{conv}}|$. J and J_{conv} are the cost function values obtained under the different simplified MPFC and the classic MPFC based on a virtual three-level space vector, respectively.

A. Simulation Results and Discussion

Fig. 7 shows the closed-loop responses under different operating speeds and torques. When an external load is applied, the four methods provide a fast dynamic torque response. At the steady-state, the proposed methods provide lower current harmonics, and also torque and flux ripples. Under reference speed change from 1430 r/min to −1430 r/min, the torque responses of the four methods are shown in subplots noted A, B, C, and D in Fig. 7. The four methods provide similar dynamic behavior.

Fig. 8 shows the different suboptimal results of DSVM-DTC ($N = 2$), 6V3-MPFC, and 3V3-MPFC methods, where J_1, J_2, J_3, J_{conv1}, and J_{conv2} represent the cost values of DSVM-DTC ($N = 2$), 6V3-MPFC, 3V3-MPFC, full-vector DSVM ($N = 2$), and V3-MPFC methods, respectively. It is seen that only the MPFC-based DB method achieves zero-suboptimality.

A comparative evaluation of the current THD, and torque and flux ripples at different operating points for the four controllers is presented in Fig. 9. Under the same sampling frequency, the traditional MPFC method provides the worst closed-loop performance. Compared with DSVM ($N = 2$), both proposed methods provide lower current THD, torque, and flux ripples.

To evaluate the range of validity of the proposed controller, various simulations for both stator and rotor under resistance, inductance, and even mutual inductance mismatches are performed. The achieved results are presented in Fig. 10. The inductance mismatch has a stronger and negative impact on the closed-loop performance compared with the resistance change. The stator resistance change has a negligible impact on the closed-loop response while the rotor resistance mismatch introduces an offset flux error and increases the torque ripples. To improve the robustness of the proposed control strategy, the observer model, the parameter identification, and model-free

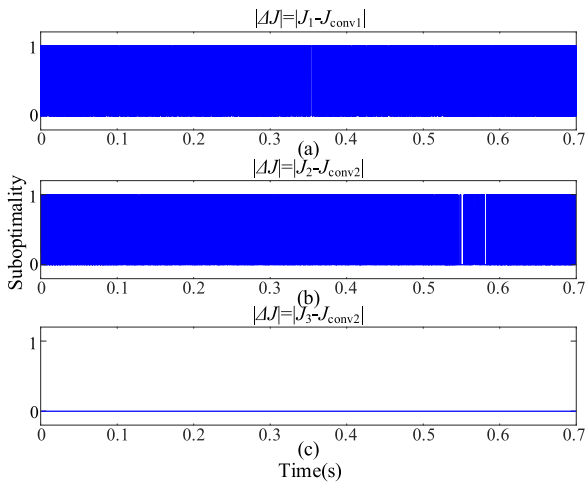

Fig. 8. Simulated suboptimization results. (a) DSVM-DTC ($N = 2$). (b) 6V3-MPFC. (c) 3V3-MPFC.

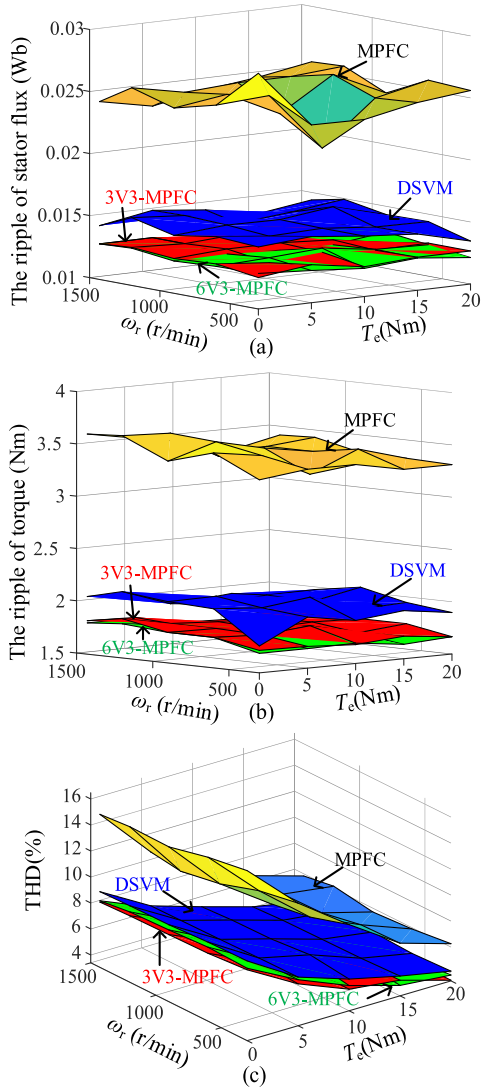

Fig. 9. Simulated steady-state response of different conditions. (a) Torque ripples. (b) Stator flux ripples. (c) Current THD.

TABLE IV
COMPUTATION BURDEN

Methods	MPFC	DSVM-DTC (N=2)	6V3-MPFC	3V3-MPFC
Estimation and delay compensation (μs)	2.15	2.15	2.15	2.15
CVVs selection (μs)	0	1.45	1.94	2.34
Prediction(μs)	13.32	13.26	10.60	5.35
RVVs selection (μs)	0.85	0.85	0.85	0.85
Others(μs)	0.95	0.95	0.95	0.95
Total(μs)	17.27	18.66	16.49	11.64
Sampling time(μs)	50	100	100	100

approaches can be studied in future work [4], [6], [28], [29], [30].

B. Experimental Results and Discussion

The structure of the experimental drive setup is shown in Fig. 11. The algorithm is implemented in the Simulink-Real-Time platform and the IM is 380 V, 3 kW, and a four-pole motor with a rated shaft speed of 1430 r/min. To evaluate the computation time of the different control strategies, a high voltage level "H" is generated during the processing of the control algorithm, and a low voltage level "L" is generated when the processing is finished or on standby for the next control period. It should be noted that, to achieve a fair comparison of the performances such as torque and flux ripples, the sampling frequency of MPFC is set as twice the value of MPFC based on an extended space vector. As shown in Fig. 12, the control period under MPFC is half the control period under other controllers.

The results summarized in Table IV show that the execution times needed for estimation and delay compensation, RVVs selection, and other steps are the same under the four controllers. The processing steps with different execution times are prediction and CVVs selection. The execution time for prediction is higher under MPFC and DSVM-DTC ($N = 2$) since both control methods evaluate a large number of VVs. The step for selecting the CVVs is more time-consuming under the 3V3-MPFC since it requires evaluating (24)–(29), and Table II.

Fig. 13 shows the responses of the four methods during speed reversal from 1430 r/min to −1430 r/min. This test confirms the effectiveness of the proposed methods under fast-speed step change. Apart from dynamic tests, the steady-state behavior of the different methods has been evaluated and compared.

The steady-state responses at rated speed and 20 Nm load are shown in Fig. 14. Even though the operating sampling frequency is twice the value under other methods, MPFC still provides higher current THD, as well as torque and flux ripples. Compared with the proposed methods, DSVM-DTC ($N = 2$) provides higher torque and flux ripples, and current THD. Furthermore, the proposed controllers require a lower computation burden. The experimental results are summarized in Table V, the two proposed controllers exhibit almost the same torque and flux ripples which are lower than the values under the classical MPFC and DSVM-DTC ($N = 2$). 3V3-MPFC provides a lower current THD and more important it reduces the execution time compared with 6V3-MPFC.

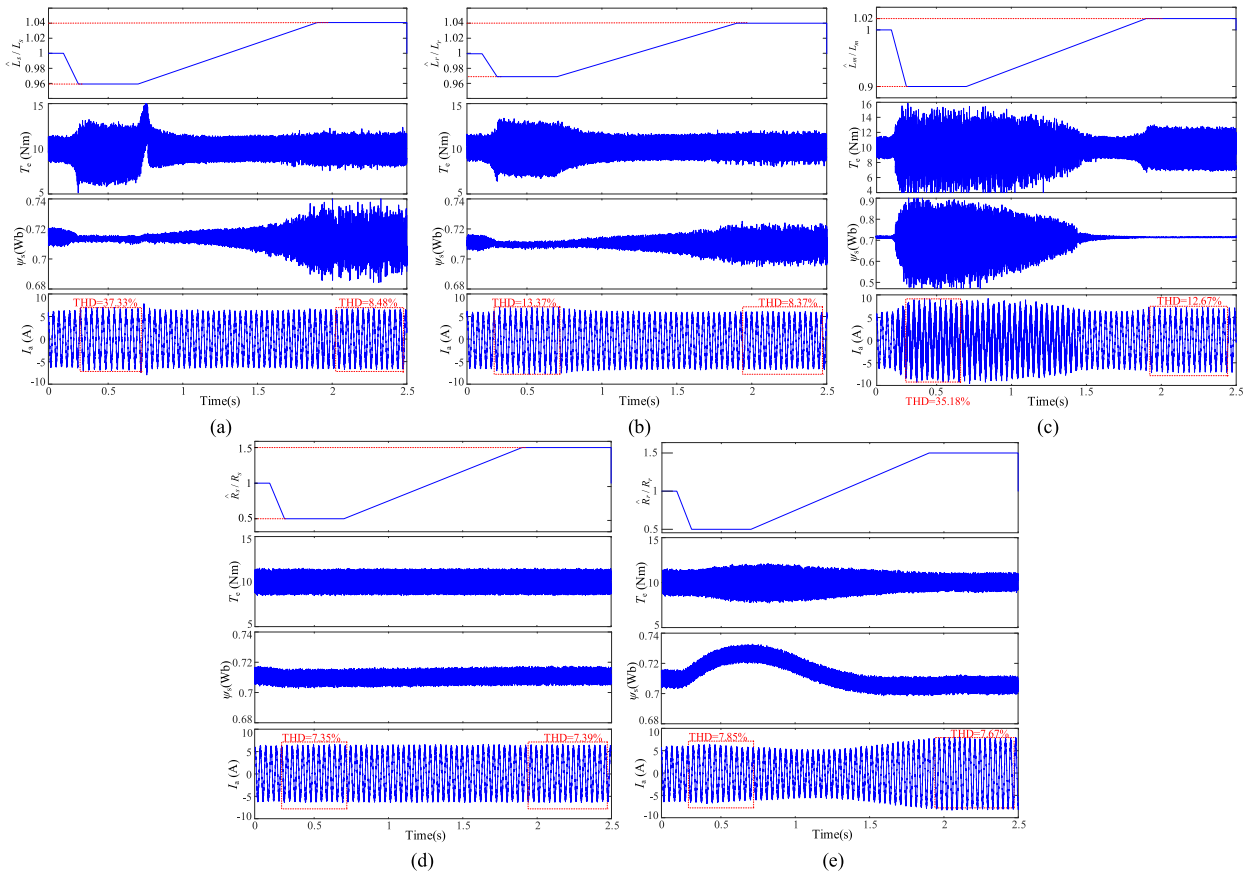

Fig. 10. Simulation results of robustness against parameters deviation at 800 r/min with 10 Nm. (a) L_s. (b) L_r. (c) L_m. (d) R_s. (e) R_r.

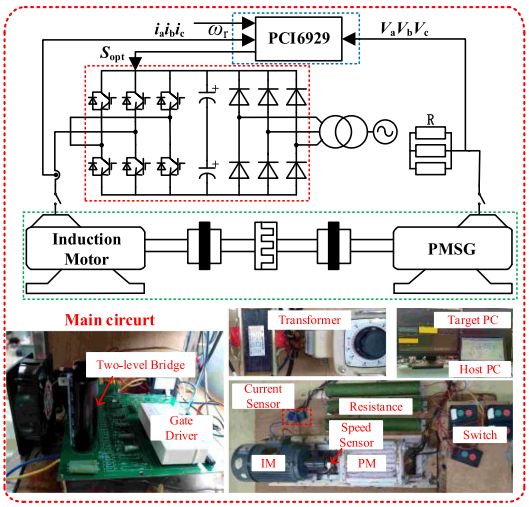

Fig. 11. Real-Time experimental platform.

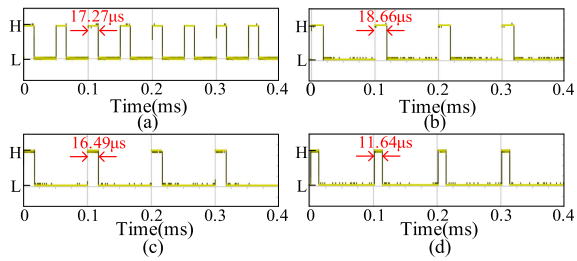

Fig. 12. Computation burden. (a) MPFC. (b) DSVM-DTC ($N = 2$). (c) 6V3-MPFC. (d) 3V3-MPFC.

TABLE V
EXPERIMENTAL STEADY-STATE COMPARISON AT 1430 R/MIN WITH 20 NM LOAD

Method	MPFC	DSVM-DTC	6V3-MPFC	3V3-MPFC
ψ_{ripple}%	1.32%	1.20%	0.95%	0.97%
T_{ripple}%	4.25%	3.71%	3.30%	3.35%
THD	8.91%	8.32%	7.30%	6.99%
ASF (kHz)	3.12	3.27	2.48	2.51

A comparative evaluation of the ASF over a wide range of operating speed and torque is presented in Fig. 15. The classical MPFC operating at 20 kHz provides an ASF between 2.6 kHz to 4 kHz, and the DSVM-DTC ($N = 2$) provides a higher ASF, which varies between 3 kHz to 4.7 kHz. The ASFs under the two proposed control algorithms are similar.

Fig. 16 shows the ASF of the 3V3-MPFC algorithm under nominal operating conditions. Without the ASF scheme, the ASF varies between 4.5 and 5.5 kHz while with the ASF scheme active, the resulting ASF varies from 2.1 to 2.8 kHz. In conclusion, suitable use of RVV effectively reduces the ASF

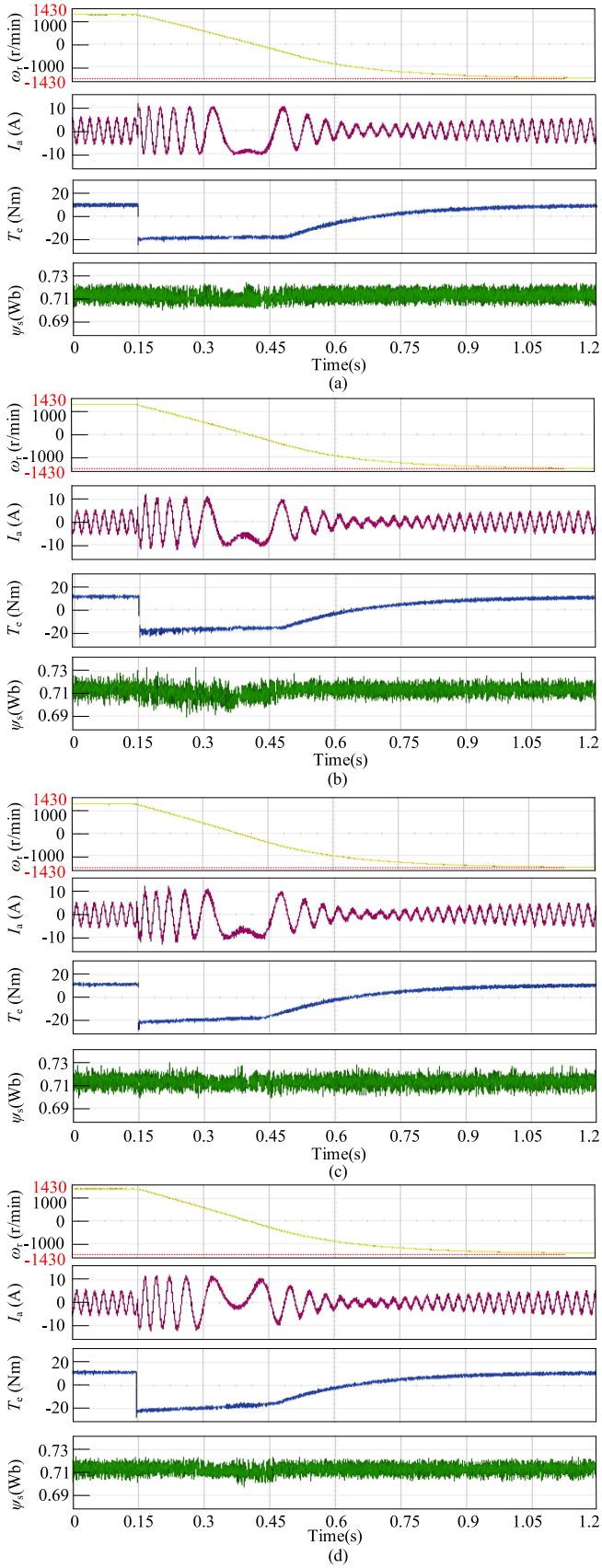

Fig. 13. Experimental response with a step change in speed from 1430 r/min to −1430 r/min. (a) MPFC. (b) DSVM-DTC ($N = 2$). (c) 6V3-MPFC. (d) 3V3-MPFC.

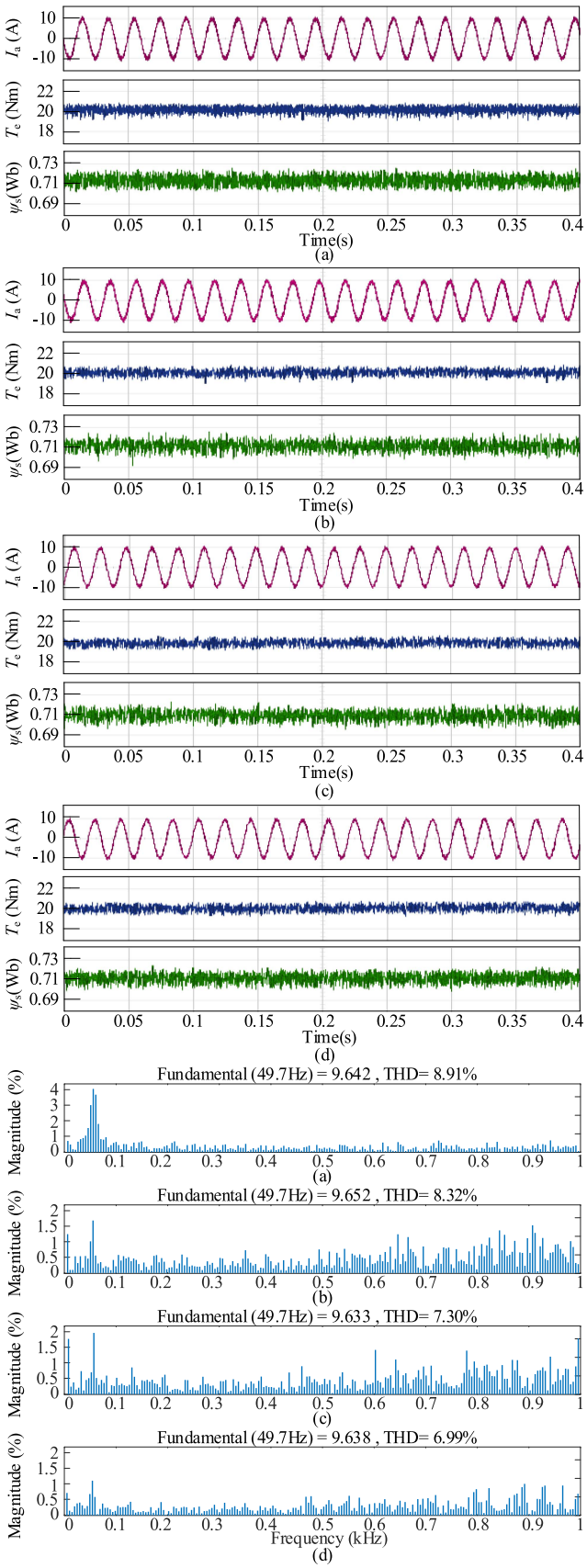

Fig. 14. Experimental response of steady-state performances at 1430 r/min with 20 Nm. (a) MPFC. (b) DSVM-DTC ($N = 2$). (c) 6V3-MPFC. (d) 3V3-MPFC.

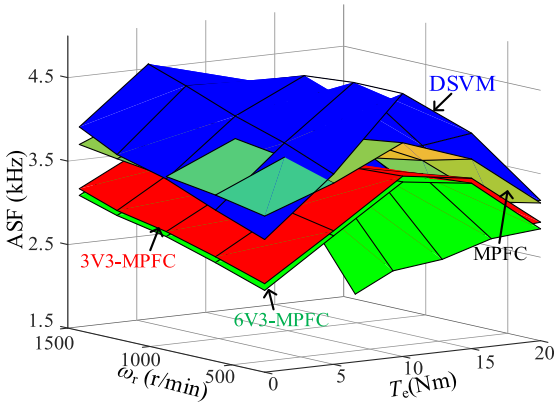

Fig. 15. ASF analysis of four methods.

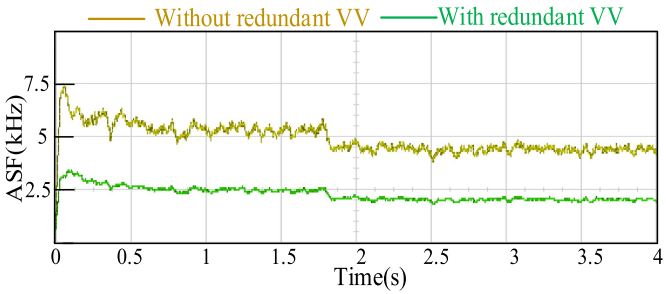

Fig. 16. ASF analysis of 3V3-MPFC at 1430 r/min with 20 Nm.

without extension of the cost function. Therefore, among the two proposed methods, the 3V3-MPFC is the most suitable solution to achieve better closed-loop performance at an acceptable operating ASF with a low-cost digital processor.

V. Conclusion

A novel MPFC has been proposed for improving the closed performances in the motor drives fed by 2L-VSI. The proposed MPFC is based on the virtual vector and the DTC/DB methods. MPFC is used to avoid flux WF, which is a limitation of MPTC; the virtual vector method is used to expand the number of state voltages and improve the MPFC closed-loop performance. To reduce the computational burden, DTC and novel DB methods are proposed to reduce the evaluation of the flux control objective to a sector and subsector, respectively. Compared with other existing methods, the new DB reduces the number of states needed and achieves a suboptimal solution that is equal to the optimal solution provided by V3-MPFC. In addition, the RVVs are exploited to reduce the ASF without extending the cost function. The simulation and experimental results show that compared with the classic MPFC and DSVM-DTC ($N = 2$), the proposed approaches provide a better steady-state response with lower torque and flux ripples, and also current THD. Most importantly, the proposed 3V3-MPFC based on the new DB requires a lower execution time, which is crucial for lowering the cost of the digital control processor.

References

[1] G. S. Buja and M. P. Kazmierkowski, "Direct torque control of PWM inverter-fed AC motors—A Survey," *IEEE Trans. Ind. Electron.*, vol. 51, no. 4, pp. 744–757, Aug. 2004.

[2] D. Casadei, F. Profumo, G. Serra, and A. Tani, "FOC and DTC: Two viable schemes for induction motors torque control," *IEEE Trans. Power Electron.*, vol. 17, no. 5, pp. 779–787, Sep. 2002.

[3] J. Rodriguez et al., "State of the art of finite control set model predictive control in power electronics," *IEEE Trans. Ind. Inform.*, vol. 9, no. 2, pp. 1003–1016, May 2013.

[4] Y. Zhang, Z. Yin, W. Li, J. Liu, and Y. Zhang, "Adaptive sliding-mode-based speed control in finite control set model predictive torque control for induction motors," *IEEE Trans. Power Electron.*, vol. 36, no. 7, pp. 8076–8087, Jul. 2021.

[5] H. Miranda, P. Cortes, J. I. Yuz, and J. Rodriguez, "Predictive torque control of induction machines based on state-space models," *IEEE Trans. Ind. Electron.*, vol. 56, no. 6, pp. 1916–1924, Jun. 2009.

[6] L. Yan and F. Wang, "Observer-predictor-based predictive torque control of induction machine for robustness improvement," *IEEE Trans. Power Electron.*, vol. 36, no. 8, pp. 9477–9486, Aug. 2021.

[7] P. R. U. Guazzelli, W. C. A. Pereira, C. M. R. Oliveira, A. G. Castro, and M. L. Aguiar, "Weighting factors optimization of predictive torque control of induction motor by multi-objective genetic algorithm," *IEEE Trans. Power Electron.*, vol. 34, no. 7, pp. 6628–6638, Jul. 2019.

[8] C. A. Rojas, J. R. Rodriguez, S. Kouro, and F. Villarroel, "Multiobjective fuzzy-decision-making predictive torque control for an induction motor drive," *IEEE Trans. Power Electron.*, vol. 32, no. 8, pp. 6245–6260, Aug. 2017.

[9] M. Norambuena, J. Rodriguez, Z. Zhang, F. Wang, C. Garcia, and R. Kennel, "A very simple strategy for high quality performance of AC machines using model predictive control," *IEEE Trans. Power Electron.*, vol. 34, no. 1, pp. 794–800, Jan. 2019.

[10] Y. Zhang, H. Yang, and B. Xia, "Model-predictive control of induction motor drives: Torque control versus flux control," *IEEE Trans. Ind. Appl.*, vol. 52, no. 5, pp. 4050–4060, Sep./Oct. 2016.

[11] Y. Zhang and H. Yang, "Two-vector-based model predictive torque control without weighting factors for induction motor drives," *IEEE Trans. Power Electron.*, vol. 31, no. 2, pp. 1381–1390, Feb. 2016.

[12] I. Osman, D. Xiao, K. S. Alam, S. M. S. I. Shakib, M. P. Akter, and M. F. Rahman, "Discrete space vector modulation-based model predictive torque control with no suboptimization," *IEEE Trans. Ind. Electron.*, vol. 67, no. 10, pp. 8164–8174, Oct. 2020.

[13] T. Jin, Y. Huang, Y. Lin, and M.-N. Daniel Legrand, "Model predictive current control based on virtual voltage vector method for parallel three-level inverters," *IEEE J. Emerg. Sel. Topics Power Electron.*, vol. 9, no. 5, pp. 6049–6058, Oct. 2021.

[14] W. Alhosaini, F. Diao, M. H. Mahmud, Y. Wu, and Y. Zhao, "A virtual space vector-based model predictive control for inherent DC-link voltage balancing of three-level T-type converters," *IEEE J. Emerg. Sel. Topics Power Electron.*, vol. 9, no. 2, pp. 1751–1764, Apr. 2021.

[15] I. Gonzalez-Prieto, M. J. Duran, J. J. Aciego, C. Martin, and F. Barrero, "Model predictive control of six-phase induction motor drives using virtual voltage vectors," *IEEE Trans. Ind. Electron.*, vol. 65, no. 1, pp. 27–37, Jan. 2018.

[16] K.-K. Shyu, J.-K. Lin, V.-T. Pham, M.-J. Yang, and T.-W. Wang, "Global minimum torque ripple design for direct torque control of induction motor drives," *IEEE Trans. Ind. Electron.*, vol. 57, no. 9, pp. 3148–3156, Sep. 2010.

[17] Y. Zhang and H. Yang, "Model predictive torque control of induction motor drives with optimal duty cycle control," *IEEE Trans. Power Electron.*, vol. 29, no. 12, pp. 6593–6603, Dec. 2014.

[18] C. Zhu, Z. Zeng, and R. Zhao, "Comprehensive analysis and reduction of torque ripples in three-phase four-switch inverter-fed PMSM drives using space vector pulse-width modulation," *IEEE Trans. Power Electron.*, vol. 32, no. 7, pp. 5411–5424, Jul. 2017.

[19] Y. Yang et al., "Low complexity finite-control-set MPC based on discrete space vector modulation for T-type three-phase three-level converters," *IEEE Trans. Power Electron.*, vol. 37, no. 1, pp. 392–403, Jan. 2022.

[20] M. Amiri, J. Milimonfared, and D. A. Khaburi, "Predictive torque control implementation for induction motors based on discrete space vector modulation," *IEEE Trans. Ind. Electron.*, vol. 65, no. 9, pp. 6881–6889, Sep. 2018.

[21] I. M. Alsofyani, N. R. N. Idris, and K. Lee, "Dynamic hysteresis torque band for improving the performance of lookup-table-based DTC of induction machines," *IEEE Trans. Power Electron.*, vol. 33, no. 9, pp. 7959–7970, Sep. 2018.
[22] J. Xu, M. Odavic, Z.-Q. Zhu, Z.-Y. Wu, and N. Freire, "Switching-table-based direct torque control of dual three-phase PMSMs with closed-loop current harmonics compensation," *IEEE Trans. Power Electron.*, vol. 36, no. 9, pp. 10645–10659, Sep. 2021.
[23] M. Habibullah, D. D. Lu, D. Xiao, and M. F. Rahman, "A simplified finite-state predictive direct torque control for induction motor drive," *IEEE Trans. Ind. Electron.*, vol. 63, no. 6, pp. 3964–3975, Jun. 2016.
[24] P. G. Ipoum-Ngome, D. L. Mon-Nzongo, J. Song-Manguelle, R. C. C. Flesch, and T. Jin, "Optimal finite state predictive direct torque control without weighting factors for motor drive applications," *IET Power Electron.*, vol. 12, no. 6, pp. 1434–1444, Feb. 2019.
[25] W. Xie et al., "Finite-control-set model predictive torque control with a deadbeat solution for PMSM drives," *IEEE Trans. Ind. Electron.*, vol. 62, no. 9, pp. 5402–5410, Sep. 2015.
[26] Y. Wang et al., "Deadbeat model-predictive torque control with discrete space-vector modulation for PMSM drives," *IEEE Trans. Ind. Electron.*, vol. 64, no. 5, pp. 3537–3547, May 2017.
[27] Y. Yang, H. Wen, M. Fan, M. Xie, and R. Chen, "Fast finite-switching-state model predictive control method without weighting factors for T-type three-level three-phase inverters," *IEEE Trans. Ind. Inform.*, vol. 15, no. 3, pp. 1298–1310, Mar. 2019.
[28] S. A. Odhano, P. Pescetto, H. A. A. Awan, M. Hinkkanen, G. Pellegrino, and R. Bojoi, "Parameter identification and self-commissioning in AC motor drives: A technology status review," *IEEE Trans. Power Electron.*, vol. 34, no. 4, pp. 3603–3614, Apr. 2019.
[29] H. Mesai Ahmed, I. Jlassi, A. J. Marques Cardoso, and A. Bentaallah, "Model-free predictive current control of synchronous reluctance motors based on a recurrent neural network," *IEEE Trans. Ind. Electron.*, vol. 69, no. 11, pp. 10984–10992, Nov. 2022.
[30] C. Ma, H. Li, X. Yao, Z. Zhang, and F. De Belie, "An improved model-free predictive current control with advanced current gradient updating mechanism," *IEEE Trans. Ind. Electron.*, vol. 68, no. 12, pp. 11968–11979, Dec. 2021.

Tao Jin (Senior Member, IEEE) received the B.S. and M.S. degrees in electrical engineering from Yanshan University, Qinhuangdao, China, in 1998 and 2001, respectively, and the Ph.D. degree in electrical engineering from Shanghai Jiaotong University, Shanghai, China, in 2005.

From 2005 to 2007, he worked as a Postdoctoral with Shanghai Jiaotong University. From 2008 to 2009, he was a Research Scientist with Virginia Tech, Blacksburg, VA, USA. In 2010, he joined Imperial College London, London, U.K., as European Union Marie Curie Research Fellow, where he focused on electrical technologies related to smart grid. He is currently a Professor with the College of Electrical Engineering and Automation, Fuzhou University, Fuzhou, China. He has authored more than 160 articles.

Dr. Jin is a Member of the IEEE Power and Energy Society and the IEEE Industrial Electronics Society, and a Special Committee Member of the Chinese Society of Electrical Engineering and the China Electrotechnical Society. He currently serves as an Associate Editor for MPCE, PCMP, China Measurement and Testing Technology, and other journals.

Huiqing Song was born in Zhejiang, China, in 1998. He received the B.S. degree in automation from Lishui University, Lishui, China, in 2020. Since 2020, he has been working toward the M.S. degree with the Department of Electrical Engineering and Automation, Fuzhou University, Fuzhou, China.

His current research interests include the model predictive control, ac motor control.

Daniel Legrand Mon-Nzongo (Member, IEEE) received the B.S. degree from the Ecole Normale Supérieure d'Enseignement Technique (ENSET), Douala University, Douala, Cameroon, in 2010, and the Ph.D. degree from Fuzhou University, Fuzhou, China, in 2018, both in electrical engineering.

From 2018 to 2021, he was a Postdoctoral Research Fellow with Pearl Electric, Co., Ltd., Guangzhou, China. During this time, he was the Team Leader of the Power Electronics Lab. He was involved on several industry funded projects related to medium-voltage converters and energy router technologies applied in railway applications. He is currently an Associate Research Professor with the College of Electrical Engineering and Automation, Fuzhou University. His current research interests include bidirectional ac and dc converters for medium voltage applications.

Paul Gistain Ipoum-Ngome (Member, IEEE) was born in Douala, Cameroon, in 1989. He received the B.S., M.S., and DEA degrees in electrical engineering from Ecole Normal Supérieure d'Enseignement Technique (ENSET), Douala University, Douala, Cameroon, in 2013, 2015, and 2016, respectively, and the Ph.D. degree in electrical engineering from Fuzhou University, Fuzhou, China, in 2021.

Since May 2021, he has been a Postdoctoral Researcher Associated with Fuzhou University and Pearl-Electric Co., Ltd., Guangzhou, China. His current research interests include MPC, data-driven predictive controller for grid-connected and motor drive applications.

Huangzheng Liao was born in Jiangxi, China, in 1998. He received the B.S. degree in electrical engineering and automation from East China Jiaotong University, Nanchang, China, in 2019. Since 2019, he has been working toward the M.S. degree with the Department of Electrical Engineering and Automation, Fuzhou University, Fuzhou, China.

His current research interests include the model predictive control, renewable power generation and control of multilevel inverters.

Minlong Zhu was born in Jiangxi, China, in 1997. He received the B.S. degree in electrical engineering and automation from Yanshan University, Qinhuangdao, China, in 2020. Since 2020, he has been working toward the M.S. degree with the Department of Electrical Engineering and Automation, Fuzhou University, Fuzhou, China.

His current research interests include the model predictive control, renewable power generation, and control of multilevel inverters.